a metallic photonic bandgap structure in a dielectric host medium, Microwave Opt Technol Lett 26 (2000), 367–371.
7. G. Poilasne, P. Pouliguen, K. Mahdjoubi, C. Terret, Ph. Gelin, and L. Desclos, Influence of metallic photonic bandgap (MPBG) materials interface on dipole radiation characteristics, Microwave Opt Technol Lett 18 (1998), 407–410.
8. G. Poilasne, P. Pouliguen, K. Mahdjoubi, J. Lenormand, C. Terret, and Ph. Gelin, Theoretical study of grating lobes reduction using metallic photonic bandgap materials (MPBGM), Microwave Opt Technol Lett 18 (1998), 32–40.
9. G. Poilasne, P. Pouliguen, J. Lenormand, K. Mahdjoubi, C. Terret, and Ph. Gelin, Theoretical study of interactions between antennas and metallic photonic bandgap materials, Microwave Opt Technol Lett 15 (1997), 384–389.
10. G. Poilasne, P. Pouliguen, K. Mahdjoubi, C. Terret, Ph. Gelin, and L. Desclos, Experimental radiation pattern of dipole inside metallic photonic bandgap material, Microwave Opt Technol Lett 22 (1999), 10–15.
11. M.M. Sigalas, R. Biswas, Q. Li, D. Crouch, R. Jacobs-Woodbury, B. Lough, S. Nielsen, S. McCalmont, G. Tuttle, and K.M. Ho, Dipole antennas on photonic bandgap crystals: Experiment and simulation, Microwave Opt Technol Lett 15 (1997), 153–158.
12. J.-M. Lourtioz, A. de Lustrac, F. Gadot, S. Rowson, A. Chelnokov, T. Brillat, A. Ammouche, J. Danglot, O. Vanbesien, and D. Lippens, Toward controllable photonic crystals for centimeter- and millimeter-wave devices, J Lightwave Technol 17 (1999), 2025–2031.
13. C.A. Balanis, Antenna theory, Wiley, New York, 1997.
14. M. Abramowitz and I. Stegun (Editors), Handbook of mathematical functions, Dover, New York, 1972.
15. A. Taflove, Computational electrodynamics: The finite-difference time-domain method, Artech House, Norwood, MA, 1995.
16. J.P. Berenger, A perfectly matched layer for the adsorption of electromagnetic waves, J Comput Phys 114 (1994), 185–200.
17. D.E. Goldberg, Genetic algorithms in search, optimization and machine learning, Addison-Wesley, Reading, MA, 1989.
18. R.E. Collin, Foundation for microwave engineering, McGraw-Hill, Singapore, 1996.

© 2001 John Wiley & Sons, Inc.

INFRARED MICROSTRIP DIPOLE ANTENNAS — FDTD PREDICTIONS VERSUS EXPERIMENT

Iulian Codreanu[1] and Glenn D. Boreman[1]
[1] School of Optics / CREOL
University of Central Florida
Orlando, Florida 31816-2700

Received 5 January 2001

ABSTRACT: *We report on the successful use of niobium microbolometers coupled to microstrip dipole antennas for the detection of midinfrared radiation. Measurements of the detector response versus antenna length performed at the 10.6 μm wavelength allowed us to identify the first three current-wave resonances along the antenna arms. The detector response was also measured as a function of the radiation wavelength in the 9–11 μm spectral domain. Excellent agreement between the experimental results and finite-difference time-domain (FDTD) predictions was obtained.* © 2001 John Wiley & Sons, Inc. Microwave Opt Technol Lett 29: 381–383, 2001.

Contract grant sponsor: Ballistic Missile Defense Organization
Contract grant sponsor: Lockheed Martin Corporation

Key words: *infrared antenna; microbolometer; microstrip dipole; FDTD method*

1. INTRODUCTION

Lithographic antenna-coupled infrared detectors were introduced during the mid-1970s [1]. Integrated infrared detectors using dipole antennas [2], bowtie antennas [3], log-periodic antennas [3], and spiral antennas [4] have been reported. In [5], we reported on the successful detection of 10.6 μm carbon dioxide (CO_2) laser radiation using an Nb microbolometer integrated with a twin rectangular microstrip patch antenna. This letter demonstrates, for the first time, the use of *microstrip* dipole antenna structures for the detection of midinfrared radiation. The difference between a printed dipole [2] and a printed microstrip dipole is that the latter is placed a fraction of a free-space wavelength above a metallic ground plane. The presence of the ground plane leads to a better confinement of the electromagnetic fields under the dipole, and thus to a higher antenna quality factor. Furthermore, for the same dielectric spacer thickness, a half-wavelength microstrip dipole has a narrower bandwidth than a rectangular microstrip patch antenna [6].

Infrared antennas are essentially scaled-down versions of their counterparts found in the microwave portion of the electromagnetic spectrum. However, as the frequency of operation increases, so does the energy dissipation within the materials involved in the fabrication of the antennas. The typical thickness of the layers that make up an antenna-coupled infrared (IR) detector is about 100 nm. The physical parameters of such thin layers depend on the details of the deposition conditions. Therefore, the material data available in the literature can only provide a starting point for the design of infrared antennas.

Full-wave electromagnetic techniques such as the method of moments (MoM), the finite-element method (FEM), and the FDTD method are well established in the RF, microwave, and millimeter-wave regions. The FDTD method, proposed by Yee in 1966 [7], solves Maxwell's curl equations by replacing the six partial differential equations with finite-difference equations. The explicit update equations obtained this way are used in a leapfrog update scheme to incrementally march the electric and magnetic fields forward in time. The accuracy of the method depends on the discretization of the spatial domain; in order to resolve the electromagnetic waves, at least ten, and up to 30 grid nodes per wavelength must be used. The method is stable as long as the time step is less than a value dictated by Courant's condition [8]. The simplicity and flexibility of this method have made it popular in solving a wide variety of problems in electromagnetics [9]. Since this algorithm uses an explicit updating scheme, very large problems can be solved using relatively inexpensive computing equipment, up to the limit of available physical memory.

Grossman et al. successfully compared MoM predictions with experimental data for dipole-antenna-coupled microbolometers at 10 μm [10]. In this letter, we demonstrate that the FDTD method can be used to extract the optical parameters of the materials used in the fabrication of antenna-coupled infrared detectors. The optical parameters of those materials were fine tuned around the values found in the literature until the FDTD predictions closely resembled the measured detector response versus antenna length. The set of optical parameters thus extracted was then used to

successfully predict the wavelength-dependent response of the detectors.

2. DEVICE FABRICATION

The microstrip-dipole antenna-coupled microbolometers were fabricated on a 3 in diameter silicon wafer. A 200-nm-thick silicon dioxide (SiO_2) layer was deposited on the polished side by plasma-enhanced chemical vapor deposition (PECVD) to provide thermal and electrical insulation between the device and the silicon wafer. A 200-nm-thick layer of evaporated gold (Au) served as the ground plane. The dielectric spacer between the dipole and the ground plane consisted of a 500-nm-thick layer of SiO_2 deposited by PECVD. After the antenna-arm pattern was defined into a layer of electron beam resist, 100 nm of Au was evaporated, followed by lift off. A thin (10 nm) layer of evaporated titanium (Ti) served as an adhesion layer between the SiO_2 and Au layers. The two antenna arms (Fig. 1) were nominally 1.8 μm wide, and were separated by a 400-nm-long gap. Antennas with full lengths ranging from 0.6 to 10.4 μm were fabricated in 0.1 μm increments. The narrow (300 nm) horizontal lines shown in Figure 1 were deposited simultaneously with the dipole antenna arms, and serve as direct current (dc) leads connecting the antenna to the biasing and read-out circuit. However, the dc leads also collect some IR radiation, and thus reduce the overall antenna polarization ratio. To alleviate this problem, the dipole antenna arms were made wider than the dc leads, taking advantage of the fact that a larger area antenna has a larger radiation cross section.

The SEM photograph shown in Figure 1 was taken before the Nb bolometer was fabricated on top of the Au antenna arms. A rectangular (1.8 μm $\times$ 1.0 μm) bolometer pattern, defined in an electron-beam resist layer, was centered on the gap between the two antenna arms. A 100-nm-thick layer of Nb was deposited by dc sputtering, and the excess metal was lifted off. The dc electrical resistance of the detectors was about 45 Ω.

3. FDTD CODES

The simulated structure consisted of a continuous gold ribbon placed on a silicon dioxide layer backed by a gold ground plane. The spatial domain was discretized using a rectangular, nonuniform computational grid. A uniaxial perfectly matched layer (UPML), introduced by Gedney [11], truncated the computation domain. The structure was excited by a numerical plane wave implemented using a total-field/scattered-field zoning of the computational domain [8]. The plane wave was normally incident on the ribbon, and was linearly polarized along the ribbon. The time dependence of the incident wave was described by a sinusoidally modulated Gaussian pulse whose spectral content spanned the 8–12 μm domain. The induced current along the gold ribbon was recorded at every time step, and the codes were run until the current completely decayed. A discrete Fourier transform (DFT) was performed "on the fly" (concurrently with the FDTD time stepping) for both the induced current and the incident wave. The DFT of the induced current was then normalized to the DFT of the incident wave.

4. RESULTS

The detectors were tested using normally incident, linearly polarized CO_2 laser radiation. The laser beam was focused by $F/1$ optics, resulting in an almost diffraction-limited spot with a $1/e^2$ radius of 13 μm and an irradiance of about 1000 W/cm^2 at focus. The detector under test was biased at 100 mV, and placed in the focus of the laser beam. A mechanical chopper modulated the laser beam at 2.5 kHz, and the change in the voltage across the terminals of the detector was recorded using a lock-in amplifier after a 10$\times$ preamplification. This signal was proportional to the change in the electrical resistance of the Nb bolometer caused by the Joule dissipation of the induced terahertz currents. Because the bolometer was placed at the center of the dipole antenna, a maximum in the induced current at that location brought about a maximum in the detector response.

Figure 2 shows the measured detector response versus dipole *full length* when the 10.6 μm CO_2 laser radiation was polarized along the antenna arms. The half-wave resonance occurs for a 1.8-μm-long microstrip dipole antenna. The first minimum in the detector response, appearing around 4.2 μm, corresponds to a full-wave antenna. The 3/2-wave resonance occurs for a 6.0-μm-long antenna.

Based on the data given in [12], the computed electrical conductivity of the gold (σ_{gold}) at 10.6 μm is 2.6×10^6 S/m. The initial values for the optical parameters of the SiO_2 ($\varepsilon_{\text{oxide}} = 4.2$, $\sigma_{\text{oxide}} = 300$ S/m) were calculated based on the

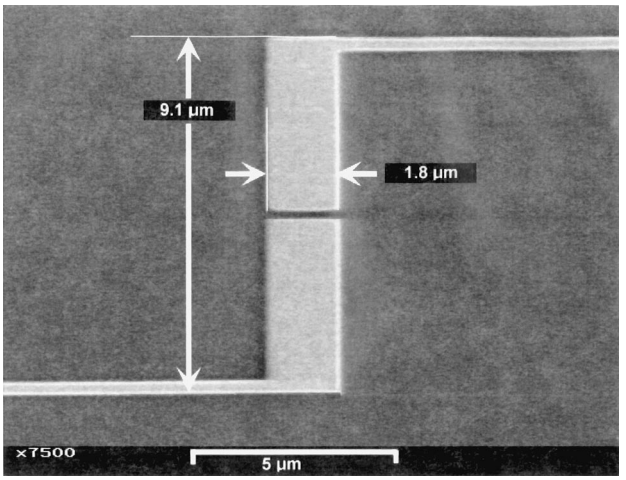

Figure 1 Top view of a microstrip dipole antenna. The electron micrograph was taken before the Nb bolometer was fabricated on top of the gold microstrip dipole antenna

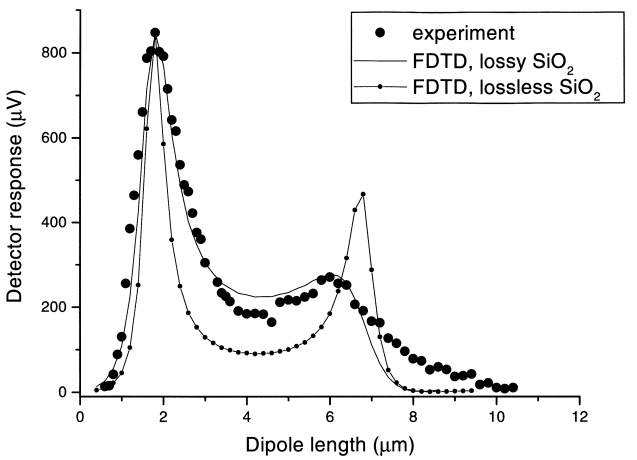

Figure 2 Detector response versus microstrip dipole antenna full length for illumination at 10.6 μm wavelength

data found in [13]. Starting with those initial values, the optical parameters of the gold and silicon dioxide were varied until the FDTD predictions closely reproduced the experimental data shown in Figure 2. The continuous line plot in Figure 2 (obtained for $\sigma_{gold} = 3.0 \times 10^6$ S/m, $\varepsilon_{oxide} = 4.0$, $\sigma_{oxide} = 700$ S/m) represents the FDTD simulated detector response. We plot the scaled squared modulus of the induced current in the middle of the Au ribbon. As can be noted, the fitted silicon dioxide loss factor is about a factor of 2 larger than the value found in the literature. The silicon dioxide was deposited by PECVD at low temperature (275°C), and is thus more porous than films grown by thermal oxidation at high temperatures (about 1000°C). The larger dielectric loss is also caused by the incorporation of impurities from the PECVD chamber (used to deposit other materials besides silicon dioxide) into the oxide film.

Figure 2 includes the FDTD predictions when the dielectric loss in the SiO_2 layer was not accounted for. As can be noted, the losses in the dielectric substrate significantly alter the response of the antenna-coupled detector.

In [2], we reported on a similar length study experiment for a set of dipoles printed on silicon substrate, but we could not precisely identify the first three (1/2-, 2/2-, and 3/2-wave) dipole resonances. The effective dielectric permittivity that we estimated there was close to that of the silicon substrate ($\varepsilon_{silicon} \approx 12.0$). Because of the lower dielectric permittivity of the SiO_2 ($\varepsilon_{oxide} = 4.0$), the resonances of the *microstrip* dipole are shifted toward longer antenna lengths compared to those of the dipoles printed on silicon. The use of SiO_2 as a dielectric substrate also increases the spacing between consecutive resonances. Also, we reduced our microstrip dipole length increment (100 nm), and we now have enough resolution to discriminate among the first three resonances.

The response of a microbolometer integrated with a 1.6-μm-long microstrip dipole antenna was measured as a function of the wavelength of the CO_2-laser radiation. Figure 3 shows the excellent agreement between the measurements and the FDTD prediction for the spectral response.

5. CONCLUSIONS

The use of an Nb microbolometer coupled to a *microstrip* dipole antenna for the detection of midinfrared radiation was demonstrated. A detector response versus antenna length study performed at 10.6 μm allowed us to identify the half-wave, full-wave, and 3/2-wave antenna current resonances. The FDTD method was used to model the experimental results. First, the optical parameters of the materials that made up the integrated detector were varied until the numerical predictions reproduced the length study experimental results. The FDTD predictions made using the fitted optical constants faithfully reproduced the detector response versus radiation wavelength measurements for a 1.6-μm-long microstrip dipole antenna. This proves that the FDTD method can be successfully used in the design and analysis of lithographic infrared antennas. The optical constants extracted by fitting the numerical simulations to the experiment will allow us more precise future designs.

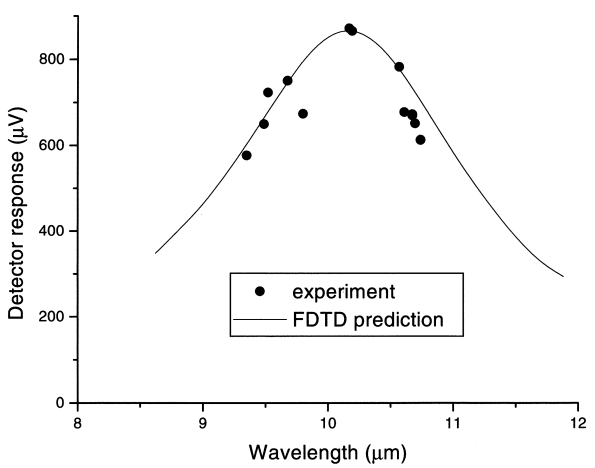

Figure 3 Detector response versus wavelength for a 1.6-μm-long microstrip dipole antenna

REFERENCES

1. S.Y. Wang, T. Izawa, and T.K. Gustafson, Coupling characteristics of thin-film metal-oxide-metal diodes at 10.6 μm, Appl Phys Lett 27 (1975), 275–279.
2. C. Fumeaux, M.A. Gritz, I. Codreanu, W.L. Schaich, F.J. Gonzalez, and G.D. Boreman, Measurement of the resonant lengths of infrared dipole antennas, Infrared Phys Technol 41 (2000), 271–281.
3. N. Chong and H. Ahmed, Antenna-coupled polycrystalline silicon air-bridge thermal detector for mid-infrared radiation, Appl Phys Lett 71 (1997), 1607–1609.
4. E.N. Grossman, J.E. Sauvageau, and D.G. McDonald, Lithographic spiral antennas at short wavelengths, Appl Phys Lett 59 (1991), 3225–3227.
5. I. Codreanu, C. Fumeaux, D.F. Spencer, and G.D. Boreman, Microstrip antenna-coupled infrared detector, Electron Lett 35 (1999), 2166–2167.
6. D.M. Pozar, Considerations for millimeter wave printed antennas, IEEE Trans Antennas Propagat AP-31 (1983), 740–747.
7. K.S. Yee, Numerical solution of initial boundary value problems involving Maxwell's equations in isotropic media, IEEE Trans Antennas Propagat AP-14 (1966), 302–307.
8. A. Taflove and K.R. Umashankar, The finite-difference time-domain method for numerical modeling of electromagnetic wave interactions, Electromag 10 (1990), 105–126.
9. A. Taflove (Editor), Advances in computational electrodynamics: The finite-difference time-domain method, Artech House, Boston, MA, 1998.
10. E.N. Grossman, J.A. Koch, C.D. Reintsema, and A. Green, Lithographic dipole antenna properties at 10 μm wavelength: Comparison of method-of-moments predictions with experiment, Int J Infrared Millimeter Waves 19 (1998), 817–825.
11. S.D. Gedney, An anisotropic PML absorbing media for FDTD simulations of fields in lossy dissipative media, Electromag 16 (1996), 399–415.
12. M.A. Ordal, R.J. Bell, R.W. Alexander, Jr., L.L. Long, and M.R. Querry, Optical properties of Au, Ni, and Pb at submillimeter wavelengths, Appl Opt 26 (1987), 744–752.
13. E.D. Palik (Editor), Handbook of optical constants of solids, Academic, New York, 1985.

© 2001 John Wiley & Sons, Inc.